

Analysis of the photoheterotrophic assimilation of valerate and associated PHA production by *Rs. rubrum*

Guillaume Bayon-Vicente^{1*}, Sarah Zarbo¹, Adam Deutschbauer², Ruddy Wattiez¹, Baptiste Leroy¹

¹ Laboratory of Proteomics and Microbiology, Research Institute for Biosciences, University of Mons, Mons, Belgium

² Environmental Genomics and Systems Biology Division, Lawrence Berkeley National Laboratory, Berkeley, California, USA

Running title

Photoheterotrophic assimilation of valerate and PHA production by *Rs. rubrum*

*Corresponding author:

Guillaume Bayon-Vicente, Laboratory of Proteomics and Microbiology, Research Institute for

Biosciences, 20 place du Parc, University of Mons, Mons, Belgium. E-mail: [guillaume.bayon-](mailto:guillaume.bayon-vicente@umons.ac.be)

vicente@umons.ac.be, phone number: +3265373311

E-mail addresses: guillaume.bayon-vicente@umons.ac.be; sarahzarbo@gmail.com;

amdeutschbauer@lbl.gov; ruddy.wattiez@umons.ac.be; baptiste.leroy@umons.ac.be.

Abstract word count: 249

Main text word count: 4966

Abstract

Purple non-sulfur bacteria are increasingly regarded for industrial applications in bioplastics, pigment and biomass production. In order to optimize the yield of future biotechnological processes, the assimilation of different carbon sources by *Rhodospirillum rubrum* (*Rs. rubrum*) has to be understood. As they are released from several fermentation processes, volatile fatty acids (VFAs) represent a promising carbon source in the development of circular industrial applications. To obtain an exhaustive characterization of the photoheterotrophic metabolism of *Rs. rubrum* in the presence of valerate, we combined phenotypic, proteomic and genomic approaches. We obtained evidence that valerate is

29 cleaved into acetyl-CoA and propionyl-CoA and depends on the presence of bicarbonate
30 ions. Genomic and enzyme inhibition data showed that a functional methylmalonyl-CoA
31 pathway is essential. Our proteomic data showed that the photoheterotrophic assimilation of
32 valerate induces an intracellular redox stress which is accompanied by an increased
33 abundance of phasins (the main proteins present in PHA granules). Finally, we observed a
34 significant increase in the production of the copolymer P(HB-co-HV) presenting an
35 outstanding (more than 80%) percentage of HV monomer. Moreover, an increase in the PHA
36 content was obtained when bicarbonate ions were progressively added to the medium. The
37 experimental conditions used in this study suggest that the redox imbalance is responsible for
38 PHA production. These findings also reinforce the idea that PNSB are suitable for PHA
39 production through another strategy than the well-known feast and famine process.

40 Importance

41
42 The use and the littering of plastics represent major issues that humanity has to face.
43 Polyhydroxyalkanoates (PHAs) are good candidates for the replacement of oil-based plastics
44 as they exhibit comparable physicochemical properties but are biobased and biodegradable.
45 However, the current industrial production of PHAs is curbed by the production costs, which
46 are mainly linked to the carbon source. Volatile fatty acids issued from the fermentation
47 processes constitute interesting carbon sources as they are cheap and easily available. Among
48 them, valerate is gaining interest regarding the ability of many bacteria to produce a
49 copolymer of PHAs. Here, we describe the photoheterotrophic assimilation of valerate by
50 *Rhodospirillum rubrum*, a purple non-sulfur bacterium mainly known for its metabolic
51 versatility. Using a knowledge based optimization process, we display a new strategy for the
52 improvement of PHA production, paving the way for the use of *Rhodospirillum rubrum* in
53 industrial processes.

1 Introduction

Rhodospirillum rubrum is a purple non-sulfur bacterium (PNSB) belonging to the α -proteobacteria group. For decades *Rs. rubrum* has been studied in order to understand the photoheterotrophic metabolism. Indeed, this bacterium is able to assimilate a broad range of carbon sources during anoxygenic photosynthesis (1,2). Among these carbon sources, volatile fatty acids (VFAs) are studied in the biotechnology field, as they are cheap and easily available. The use of the by-products issued from the fermentation bioprocesses could also increase the circularity of the bioindustry (3–5). As acetic acid is the most abundant VFA resulting from the fermentation processes, its assimilation has been broadly studied (6–12). It is now well accepted that, in isocitrate lyase gene lacking organisms (*icl*)(13), such as *Rs. rubrum*, an alternative pathway, the ethylmalonyl-CoA pathway (EMC) is used(11) for acetate photoassimilation. The role of this pathway was first characterized by Alber's group(9,10). Beside the EMC pathway, the use of additional metabolic routes, such as the isoleucine biosynthesis and degradation pathways (MBC pathway) or the pyruvate ferredoxin oxydoreductase (PFOR), remains obscure and further studies are still needed to attest to their involvement in acetate assimilation (11,12,14,15) .

Valerate constitutes the fourth most abundant VFA resulting from the majority of fermentation processes (16,17). However, some studies have revealed that the fermentation of pig feces resulted in equal proportions of each VFA, or an even higher proportion of valerate than the other VFAs (18). Moreover, some processes deliberately enriched their fermentation effluent with valerate in order to induce the production of the polymer (poly(3-hydroxybutyrate-*co*-3-hydroxyvalerate)) P(HB-*co*-HV) (19) which possesses more interesting physicochemical properties than PHB (*e.g.* higher elasticity, flexibility,...). This further demonstrates the importance of understanding the photoheterotrophic assimilation of this VFA

79 by *Rs. rubrum*. Despite this interesting feature, few studies related to the photoheterotrophic
80 assimilation of valerate are available (20). In this study by Janssen and Harfoot, it was stated
81 that all *Rhodospirillaceae* were able to photoassimilate valerate, but no information was given
82 about the underlying metabolic pathway. In *Escherichia coli*, the assimilation of valerate has
83 been reported to rely on the ATO system responsible for short chain fatty acid degradation
84 (21).

85 The use and littering of petroleum-based plastics is one of the major issues that
86 humanity faces. Polyhydroxyalkanoates (PHAs) represent good candidates to replace
87 conventional plastics as they exhibit physicochemical properties close to oil-based plastics
88 (22–24) with the advantage of being biobased and biodegradable (25,26). However, the
89 production costs today still limit the economic sustainability of the PHA industry. In some
90 processes, the carbon source may account for more than 50% of the total production costs
91 (27). The use of cheap substrates, such as VFAs, may thus represent a way to significantly
92 decrease these costs. Moreover, the nature of the carbon source influences the type and
93 composition of the PHAs produced. In this context, the use of carbon sources with an odd
94 number of carbons, such as propionate or valerate, is known to induce the production of the
95 co-polyester poly-3-hydroxybutyrate-co-3-hydroxyvalerate (P(3HB-co-3HV)) (28,29) which
96 exhibits enhanced physicochemical properties with a higher elasticity and lower melting point
97 and crystallinity(26).

98 In this paper, we investigate valerate assimilation by *Rs. rubrum* S1H using global
99 analyses of the metabolism (proteomic and functional genomic approaches) and targeted
100 analyses using knock out mutant and chemical inhibition of key enzymes. Our results
101 demonstrate that the presence of bicarbonate ions is mandatory for the assimilation of
102 valerate. We also show that valerate is first cleaved into propionyl-CoA and acetyl-CoA. Our
103 whole metabolism analyses reveal that a fully functional methylmalonyl-CoA pathway is

104 mandatory for the photoheterotrophic assimilation of valerate and that the ethylmalonyl-CoA
105 pathway is not necessary for the assimilation of acetyl-CoA issued from valerate cleavage.
106 We suggest that other pathways, such as pyruvate ferredoxin oxydoreductase (PFOR) or
107 isoleucine biosynthesis may take part in this assimilation process as has already been
108 suggested by our previous studies (11,12,14,15). We also investigate PHA production by *Rs.*
109 *rubrum*, highlighting the production of copolymers with an outstanding HV monomer
110 percentage, even in conditions of full nutrient availability. We finally highlight the capacity of
111 controlling the composition of polymers by the sequential addition of VFAs, which would
112 represent a major advance in controlling the production of biopolymers.

113 2. Materials and methods

114 2.1 Bacterial strain, medium composition and cultivation 115 conditions 116

117 The strain *Rhodospirillum rubrum* S1H (ATCC25903) as well as the $\Delta ccr::km^R$
118 strain were cultivated in medium as previously described (11,12). The medium was
119 supplemented with valerate (24.9 mM) as a carbon source, NH_4Cl (35 mM) as a nitrogen
120 source, biotin (0.06 mM) and a defined amount of added bicarbonate (3 or 50 mM). Stock
121 cultures were cultivated in a supplemented malate ammonium (SMN) rich medium. The
122 precultures used here were all cultivated in the presence of succinate as a carbon source.
123 Cultures were submitted to 50 μmol photons/ m^2 s (Sencys; 10 W; 100 lumens; 2,650 K).
124 The upper gaseous phase was flushed using pure N_2 and flasks were hermetically sealed.

125 Growth was followed through optical density (OD_{680nm}) measurement.
126 *Rhodospirillum rubrum* was cultivated under anaerobic phototrophic conditions. Cultures
127 were inoculated at a starting OD_{680nm} between 0.450 and 0.550 and incubated at 30°C with
128 rotary shaking at 185 rpm. Five clonal biological replicates were used for each culture

129 condition. Cell dry weight was approximated using a standard (conversion factor: CDW=
130 $0.6521 \times \text{OD}_{680\text{nm}}$).

131 **2.2 Mutant strain control**

132

133 The presence of *ccr* and *kmR* cassette genes in both the WT and mutant strain was
134 verified through PCR and electrophoresis gel. Genomic DNA (RNA-free) was isolated
135 from 500 μl of bacterial culture using the QIAamp DNA Mini Kit (QIAGEN) according
136 to the manufacturer's instructions. The concentration and quality of the isolated DNA
137 samples were measured using a BioSpec-Nano (Shimadzu) micro-volume
138 spectrophotometer based on UV spectra. The samples were adjusted to a concentration of
139 1 ng/ μl . Extracted DNA was then submitted to PCR using a specific primer for Crotonyl-
140 CoA reductase/carboxylase (Ccr-Rru_A3063) and Kanamycin Resistance gene (KmR)
141 (12). DNA was then submitted to electrophoresis and the presence of the targeted genes
142 was revealed using Gel Red.

143 **2.3 Monitoring the carbon source concentration in the medium**

144

145 Culture supernatants were obtained from culture samples after centrifugation at 16,000
146 g for 10 min at 4°C using a Shodex Sugar SH1011 column (300 mm x 8 mm) with aqueous
147 H_2SO_4 (0.01N) as the mobile phase, as previously described (11). Valerate and succinate
148 concentrations were determined by the integration of their specific peak and comparison with
149 a reference curve prepared with the corresponding standard. Detection was performed using a
150 refractometer.

151 **2.4 Polyhydroxyalkanoate extraction and quantitation**

152

153 PHAs were isolated as previously described (30) with some modifications. Briefly 500
154 μl of culture were centrifuged (8000 rpm, 15 minutes) and stored at -20°C until analysis.

155 PHAs were extracted and methanolysed by resuspending pellets in 500 μ l of chloroform and 2
156 mL of methanolysis solution consisting of UHPLC methanol: concentrated HCl (90:10). The
157 methanolysis solution also included 0.1 mg/ml of 3-methylbenzoic acid as an internal
158 standard. The mixture was then incubated at 100°C for 2 hours before being cooled on ice. 2
159 mL of distilled water was then added and the bottom chloroformic part was recovered and
160 analyzed by GC-MS (Shimadzu GC-MS QP2010S).

161

162 **2.5 Mutant fitness assay**

163

164 The mutant library was produced following the protocol described by Wetmore *et*
165 *al.*(31) and described in De Meur *et al.* (12).

166 The mutant fitness assays were performed in five replicates starting with five different
167 glycerol stocks of the mutant library. Each aliquot of the mutant library was independently
168 recovered in SMN with 50 μ g/ml kanamycin under dark aerobic conditions. The recovered
169 library was rinsed and resuspended in defined medium to reach a starting OD_{680nm} of 0.1.
170 Samples of biomass were collected at “time zero” (before growth selection) and after five
171 generations of growth in the selected condition, and the genomic DNA was extracted using
172 the QIAamp DNA Mini Kit (Qiagen). The concentration and purity of the extracted DNA
173 were assessed with a BioSpec-Nano (Shimadzu Biotech) before storage at -80°C. We
174 performed DNA barcode sequencing (BarSeq) as described by Wetmore *et al.*(31) to quantify
175 the barcodes and, consequently, the abundance of each mutant in each experimental condition.
176 The strain fitness was determined as the normalized log₂ ratio of bar code counts between
177 samples after five generations and the “time-zero” reference samples. Gene fitness was
178 calculated as the weighted average of the individual strain fitness values for a given gene, as
179 described. Only genes exhibiting fitness value below -0.5 were considered for further
180 analysis.

181 **2.6 Proteomic analysis**

182
183 Bacteria were harvested via centrifugation (16,000 g, 4°C) at the beginning of the
184 exponential phase (OD_{680nm} :0.9-1). Proteins were extracted using guanidinium chloride (6 M)
185 and ultrasonication (3*10 sec, IKA U50 sonicator (Staufen, Germany), amplitude 40%).
186 Protein concentration was determined using the Bradford method(32) with Bovine Gamma
187 Globulin as standard. 50 µg of proteins were reduced (DTE), alkylated (iodoacetamide) and
188 finally precipitated overnight using acetone. The obtained protein pellets were then
189 solubilized using 50 mM ammonium bicarbonate containing 1 µg of trypsin and incubated
190 overnight at 37°C. Digestion was stopped by adding 0.1% formic acid (v/v, final
191 concentration).

192 Protein identification and quantification were performed following a label-free strategy
193 on a UHPLC HRMS platform (Eksigent 2D ultra-AB SCIEX TripleTOF™ 5600). Peptides (2
194 µg) were separated in a 25 cm C18 column (Acclaim PepMap100, 3 µm, Dionex) using a
195 linear acetonitrile (ACN) gradient [5-35% (v/v), in 120 min] in water containing 0.1% (v/v)
196 formic acid at a flow rate of 300 nl.min⁻¹. Data were acquired in a data-dependent acquisition
197 mode (DDA). Search parameters included differential amino acid mass shifts for
198 carbamidomethyl cysteine, oxidized methionine, all biological modifications, amino acid
199 substitutions and missed trypsin cleavage sites. ProteinPilot Software (v4.1) was used to
200 perform database searches against the UniProt database, restricted to *Rhodospirillum* entries
201 (ATCC11170). The areas under the XIC curves of peptides were computed using
202 PeakView™ 2.1 (ABSciex, USA) and individually normalized based on a summed area of all
203 peptides for each sample. Five biological replicates were considered for each condition.
204 Markerview™ 1.2.1 (ABSciex, USA) was used for the statistical treatment of the data.

205 All computed data, as well as raw data, were uploaded to the MassIVE repository and are
206 freely accessible (dataset identifier: MSV000085300)
207 <https://massive.ucsd.edu/ProteoSAFe/dataset.jsp?task=b5561aeb53f940248f6032205e12e014>

208 3. Results and discussion

209 3.1 Bicarbonate ions are necessary for the photoheterotrophic assimilation 210 of valerate 211 212

213 In order to first characterize the photoheterotrophic assimilation of valerate,
214 *Rhodospirillum rubrum* S1H (*Rs. rubrum*) was cultivated with valerate as the sole source of
215 carbon. As bicarbonate ions are already known to act as a limiting factor in VFA assimilation
216 such as acetate, propionate or butyrate (12,14,33–35), we tested the effect of an addition of a
217 low and high concentration of bicarbonate ions (3 and 50 mM HCO_3^-) in the medium and
218 used succinate as the control condition. Indeed, previous studies have demonstrated that
219 bicarbonate ions are necessary during VFA assimilation to handle redox stress through the
220 activation of a redox sink, namely the Calvin-Benson-Bassham cycle (34,36,37). Moreover,
221 we have previously shown that bicarbonate ions are necessary for *Rs. rubrum* growth under
222 high light intensity (15). As shown in Fig. 1A, the phototrophic growth of *Rs. rubrum* with
223 valerate as the sole carbon source, and supplemented with a low concentration of bicarbonate
224 ions, stopped at an $\text{OD}_{680\text{nm}}$ of 1.5 ± 0.2 , whereas growth with a high concentration of
225 bicarbonate ions reached an $\text{OD}_{680\text{nm}}$ of 5.9 ± 0.1 (Fig. 1A). Interestingly, an identical carbon
226 supply (124 mM of C equivalent and 50 mM HCO_3^-) led to higher biomass production in the
227 presence of valerate than in the presence of succinate (calculated biomass concentration: Val
228 = 3.73 mg/mL vs Succ = 2.40 mg/mL). Indeed, 1.79 ± 0.08 mg of biomass were accumulated
229 per mg of available carbon in the presence of valerate, whereas 1.48 ± 0.03 mg of biomass
230 were accumulated per mg of available carbon in the presence of succinate (p-value < 0.001),

231 suggesting a significant assimilation of bicarbonate ions under valerate condition. In order to
232 attest to the essentiality of bicarbonate ions during photoheterotrophic growth with valerate as
233 the sole source of carbon, *Rhodospirillum rubrum* was cultivated in the presence of valerate
234 with only 3 mM of added bicarbonate ions. As expected, the growth stopped around OD_{680nm}
235 ~ 1.5. Once growth stopped, 10 mM of bicarbonate ions (final concentration) were added to
236 the culture and growth was monitored. The growth immediately restarted after this addition of
237 bicarbonate ions, reaching a final OD_{680nm} comparable to those observed with high
238 bicarbonate supplementation (Fig. 1B). The essentiality of bicarbonate ions for the
239 assimilation of acetate, propionate or butyrate has already been documented(14,15,34,38). As
240 the valerate constitutes the most reduced VFA compared to the biomass (redox state valerate:-
241 2.5; biomass: -0.5)(39,40), the requirement of bicarbonates ions could be linked to the redox
242 stress induced by the photoheterotrophic assimilation of valerate.

243 Consistently, proteomic analysis revealed that the Ribulose 1,5-Bisphosphate
244 Carboxylase/Oxygenase (RuBisCO), the main enzyme of the Calvin-Benson-Bassham (CBB)
245 cycle, was more abundant (Rru_A2400; fold change = 1.71, *p*-value = 0.01, # peptides = 89)
246 during the photoheterotrophic assimilation of valerate compared to succinate. This
247 observation further corroborates the strict necessity of bicarbonate ions for the assimilation of
248 valerate and the higher biomass productivity. Moreover, the mutant fitness assay showed that
249 a functional CBB cycle was essential in both conditions, as already demonstrated for
250 succinate (37). This observation corroborates the results obtained during the phenotypic
251 analyses. Considering this observation, it seems that HCO₃⁻ is, at least partly, consumed
252 through the Calvin-Benson-Bassham cycle, suggesting a role of this pathway in the
253 dissipation of the reduced equivalents generated during the photoheterotrophic assimilation of
254 valerate.

3.2 The photoheterotrophic assimilation of valerate induces a cellular redox stress and an increased PHA production

The proteomic analysis showed the higher abundance of four proteins related to stress handling and redox homeostasis in the presence of valerate. Unfortunately, only one of the genes encoding for these proteins (stress protein, *rru_A0894*) was present in our mutant fitness dataset. The analysis of the fitness value for this gene revealed that it was essential in both conditions (Table 1). Beside proteins implicated in redox homeostasis, proteomic analysis also revealed a higher abundance of proteins involved in the metabolism of PHAs, such as phasins in the presence of valerate. One the two phasins quantified in the proteomic analysis (*Rru_A2817*) exhibited a large fold change of 48.24 compared to succinate condition. The second phasin (*Rru_A3283*) was found to be twice more abundant in the presence of valerate than under the succinate condition (fold change = 2.06, *p*-value = 0.027, # peptides = 80). We also highlighted the higher abundance of the uncharacterized protein *Rru_A2111* (fold change = 3.56, *p*-value = 2.24E-06, # peptides = 27) which was recently described as potential phasin by Narancic *et al* (41). Nevertheless, the exact role of these proteins remains unclear as they exhibit both a function in PHB granule mobilization and a role in increasing the number of PHB granules in a cell (42). Moreover, the polyhydroxyalkanoate depolymerase (*Rru_A3356*), responsible for the degradation of PHA, showed a lower abundance compared to the succinate condition (Table 1).

Conversely to the proteomic results, which suggest the involvement of PHA synthesis in the adaptation of *Rs. rubrum* to the growth with valerate as the sole carbon source, none of the genes coding for the abovementioned proteins were observed as essential for the photoheterotrophic assimilation of valerate in the genome-wide mutant fitness assay. This may be explained by the addition of a high concentration of bicarbonate ions in the medium used to perform this experiment. Indeed, both the PHA production and the CBB cycle are

281 known to act as electron sinks (15,34,36,37,43–46). This therefore suggests that PHA
282 production may be not essential as long as another electron sink metabolism, such as the CBB
283 cycle, is available. Moreover, the genes may also be redundant in the genome which means
284 that the loss of a single gene will not lead to a specific phenotype. Interestingly, genes coding
285 for enzymes involved in the conversion of acetyl-CoA into (S)-3-hydroxybutyryl-CoA were
286 highlighted as essential for the phototrophic assimilation of valerate by *Rs. rubrum*. One of
287 these enzymes, the 3-hydroxybutyryl-CoA dehydrogenase (Rru_A3079), is known to
288 consume reduced equivalents (Fig. 2, see supplementary Table 1) and might thus take part in
289 the handling of the redox equilibrium.

290 The higher abundance of phasins combined with a lower abundance of PHA
291 depolymerase highlighted by the proteomic results suggests an increased production of PHA
292 in valerate conditions. Moreover, the mutant fitness assays showed that the (S)-3-
293 hydroxybutyryl-CoA dehydrogenase was essential in the presence of valerate. In order to
294 validate the increased PHA production during valerate assimilation, the PHA content of the
295 biomass was monitored along the growth curve under valerate and succinate conditions. As
296 expected, an increased PHA production was observed during photoheterotrophic growth of
297 *Rs. rubrum* in the presence of valerate (reaching up to 14.20 ± 1.37 % of the biomass dry
298 weight after 30 hours of culture) (Fig. 3A) whereas the PHA content was under the limit of
299 detection under succinate condition (data not shown). The abundance of PHA produced under
300 valerate was rather low. Indeed, Cerrone *et al.* performed PHA content analyses on *P. putida*
301 and observed that this bacterium was able to accumulate from 19 to 24 % of PHA CDW in the
302 presence of valerate as the sole carbon source (47). We hypothesized that PHA production
303 was used as an electron sink and that its production could be curbed by other electron sinking
304 processes. As such, the presence of bicarbonate ions and their assimilation through the
305 Calvin-Benson-Bassham cycle could represent a major competitor pathway to PHA

306 production. Indeed, proteomic and mutant fitness assay data showed that the CBB cycle was
307 probably involved in the metabolism of valerate. Therefore, we attempted to reduce the level
308 of HCO_3^- in the cultures in order to reduce the electron sink role of the CBB cycle as much as
309 possible. Cultures were started in valerate containing medium with a low concentration of
310 HCO_3^- (3mM) which was only resupplied (up to 3mM in the medium) when a growth arrest
311 was observed. This resulted in a sequential growth behaviour restarting each time we added
312 bicarbonate ions in the medium (Fig. 3B). Each addition of HCO_3^- was thus preceded by a
313 growth arrest and a reduced valerate uptake rate. Interestingly, each of the transient stationary
314 phases this procedure created was characterized by an increase of the intracellular PHA
315 content (Fig. 3B). By starving the CBB cycle of bicarbonate ions, *Rs. rubrum* accumulated up
316 to $22.57 \pm 5.89\%$ of the cell dry weight after 70 hours of culture. Indeed, this content
317 significantly increased during the first transient stationary phase (T: 27h; PHA: $10.86 \pm 2.58\%$
318 CDW; T: 70h; PHA: $22.57 \pm 5.89\%$ CDW, $p\text{-value} < 0.05$). The second transient stationary
319 phase, which corresponded to the second bicarbonate starvation of the culture (T: 101h), was
320 also accompanied by a significant ($p\text{-value} < 0.05$) PHA content increase of 133% rising from
321 $7.98 \pm 1.94\%$ (T101h) to $18.61 \pm 2.94\%$ (T174h) CDW (Fig. 3B). Interestingly, the PHA
322 content obtained after both stationary phases was significantly higher ($p\text{-value} < 0.05$) than the
323 PHA content observed in the presence of excess HCO_3^- (PHA_{excessHCO3-}: $14.20 \pm 1.37\%$;
324 PHA_{3mMfirst stationary phase}: $22.57 \pm 5.89\%$; PHA_{3mMsecond stationary phase}: $18.61 \pm 2.94\%$, $p\text{-value} <$
325 0.05). In opposition to what is usually observed (48–52), PHA increased production is not
326 triggered through a feast and famine process, suggesting that PHA production could be linked
327 to an intracellular redox imbalance. Indeed, the depletion of bicarbonate ions in the medium
328 represents a non-favorable redox environment for *Rs. rubrum* cultivated in the presence of
329 valerate. The concomitant increase in the PHA content and its further mobilization after
330 HCO_3^- repletion demonstrates that PHAs are produced by *Rs. rubrum* to deal with the redox

331 imbalance imputed to the photoheterotrophic assimilation of valerate as already hypothesized
332 (15,44,46).

333 **3.3 Acetyl-CoA and propionyl-CoA assimilation pathways highlighted as** 334 **potential pathways involved in the photoheterotrophic assimilation of** 335 **valerate**

336 **3.3.1 β -oxidation as a first step of the photoheterotrophic assimilation of valerate** 337

338 The literature suggests that following its activation into valeryl-CoA, valerate (C5) is
339 cleaved into acetyl-CoA (C2) plus propionyl-CoA (C3) through β -oxidation (21,53). As such,
340 we searched our proteomic and mutant fitness dataset for β -oxidation related proteins or genes
341 respectively. The mutant fitness analysis revealed the importance of the genes *rru_A1308*,
342 *rru_A3801*, *rru_A1309* and *rru_A1310* coding for an acyl dehydrogenase, enoyl dehydratase,
343 3-hydroxyacyl-CoA dehydrogenase and acetyl-CoA-C-acyltransferase respectively for
344 optimal fitness during valerate photoheterotrophic assimilation (significance threshold: -0.5;
345 *rru_A1308*: fitness value Succ: 0.03, Val: -0.52; *rru_A3801*: fitness value Succ: -0.25, Val: -
346 0.92; *rru_A1309*: fitness value Succ: -0.18, Val: -1.00 and *rru_A1310*: fitness value Succ:
347 0.10, Val: -0.72). Collectively, these enzymes may link the valerate uptake to the production
348 of acetyl-CoA and propionyl-CoA. However, further investigations are required to understand
349 the absence of change in the abundance or even the downregulation highlighted by the
350 proteomic analysis for these enzymes (*Rru_A1308*: *p*-value: 0.16, fold change Val/Succ: 0.77;
351 *Rru_A3801*: *p*-value: 0.51, fold change Val/Succ: 1.11; *Rru_A1309*: *p*-value: 0.0035, fold
352 change Val/Succ: 0.65; *Rru_A1310*: 0.00075, fold change Val/Succ: 0.49).

353

354 **3.3.2 Acetate related pathways are highlighted through proteomic analysis for the** 355 **photoheterotrophic assimilation of valerate** 356

357 The proteomic data revealed that several enzymes already associated with the acetate
358 metabolism, such as the enzymes of the ethylmalonyl-CoA (EMC) pathway (Rru_A3062, fold
359 change = 1.65, p -value = 0.05, #peptides = 9; Rru_A3063, fold change = 6.35, p -value =
360 0.00012, #peptides = 26; Rru_A3064, fold change = 2.53, p -value = 0.01, #peptides = 42) or
361 the pyruvate ferredoxin oxydoreductase (PFOR) (Rru_A2398, fold change = 1.51, p -value =
362 0.04, #peptides = 125) (Fig. 2), were differentially regulated in the presence of valerate and
363 could also be involved in the photoassimilation of valerate. The EMC pathway was shown to
364 be essential for the photoheterotrophic assimilation of acetate by our group (11,12) as well as
365 others (9,10) and it is now established that this pathway acts as an anaplerotic pathway during
366 the phototrophic assimilation of acetate. PFOR is known to convert acetyl-CoA into pyruvate
367 and has also been highlighted by previous proteomic analyses (2,11,12,54,55) in the presence
368 of acetate. Besides proteins for which their implication in acetate assimilation has been well
369 established, the proteomic analysis revealed the higher abundance of proteins belonging to the
370 branched chain amino acid (BCAAs) biosynthesis and degradation pathways, which represent
371 a more controversial assimilation pathway (Rru_A0468, fold change = 2.18, p -value = 0.05,
372 #peptides = 9; Rru_A0469, fold change = 1.61, p -value = 0.01, #peptide =42; Rru_A2223,
373 fold change =4.95, p -value = 0.016, #peptides = 24; Rru_A1946, fold change = 1.74, p -value
374 = 0.04, #peptides = 2; MerR transcription regulator Rru_A1994, fold change = 1.75, p -value =
375 0.04, #peptides= 4) (Fig. 2). The implication of BCAA biosynthesis and degradation
376 pathways have already been proposed as potential assimilation pathways in the presence of
377 butyrate (14) or acetate (11,12). Recently, a sudden increase in light intensity highlighted that
378 isoleucine biosynthesis may be implicated in high light intensity tolerance (15), further
379 reinforcing the implication of this pathway in managing the redox balance as already
380 proposed (56,57). This latter hypothesis is supported by the present redox issue observation
381 but would require further dedicated research.

382 However, contrary to what was observed in the proteomic data, the genome-wide
383 mutant fitness assay revealed that the ethylmalonyl-CoA pathway was not essential for
384 valerate photoassimilation by *Rhodospirillum rubrum* (Fig. 2, see supplementary table 1). It
385 could indicate that the observed upregulation of the enzyme of the EMC could be imputed to
386 the side regulation of the EMC pathway due to the presence of acetyl-CoA following the
387 cleavage of valerate, but that this pathway is not extensively used during valerate
388 photoassimilation.

389 In order to clearly address the essentiality of the EMC pathway, we cultivated a
390 $\Delta ccr:km^R$ mutant strain (lacking the gene coding for the key enzyme of the EMC pathway, see
391 Fig. 2) in the presence of valerate as the sole source of carbon. It revealed that the EMC
392 pathway was not essential for the growth of *Rs rubrum* in the presence of valerate (Fig. 4A)
393 confirming the genome-wide mutant fitness assay. The genotype of the mutant strain was
394 confirmed using PCR analysis (see supplementary figure 1).

395 **3.3.2 The methylmalonyl-CoA pathway is essential for the photoheterotrophic**
396 **assimilation of valerate**
397

398 The assimilation of valerate through acetyl-CoA and propionyl-CoA involves that a
399 higher activity of the propionyl-CoA assimilation pathway (the methylmalonyl-CoA pathway-
400 MMC) (58–60) should be observed under valerate conditions. However, enzymes of the
401 MMC pathway were not upregulated under valerate conditions, as revealed by the proteomic
402 analysis. Many researchers have already observed that propionyl-CoA could be formed from
403 succinate (61–63), which could impair the detection of an increased abundance of enzymes of
404 the MMC pathway. Interestingly, the mutant fitness analysis highlights that the two subunits
405 of two proteins implicated in the propionyl-CoA assimilation pathway, the propionyl-CoA
406 carboxylase and the methylmalonyl-CoA mutase (*rru_A0052*; *rru_A0053*; *rru_A2479* and
407 *rru_A2480*), are essential for optimal fitness for the phototrophic assimilation of valerate, but

not of succinate (Fig. 2, see supplementary table 2). These genes have already been shown to be essential for propionyl-CoA assimilation (58,64,65). These results suggest that the production of propionyl-CoA represents a major step for valerate assimilation. One hypothesis explaining the essentiality of MMC, but not of EMC, is that the propionyl-CoA assimilation pathway could represent an anaplerotic pathway for the TCA cycle as it yields succinate, EMC being no more essential to filling this role. In order to attest to the essential role of the methylmalonyl-CoA pathway in valerate assimilation, itaconic acid was used to inhibit the propionyl-CoA carboxylase (Rru_A0052/A0053, see Fig. 2) (64). Growth of *Rs. rubrum* in the presence of succinate as the main source of carbon and 20 mM of itaconic acid confirmed the absence of toxicity of itaconate, as already shown by Berg *et al.* (64). As presented in Fig. 4B, the addition of 20 mM of itaconic acid impaired the growth of *Rs. rubrum* in the presence of valerate, both for the wild-type strain and for the $\Delta ccr::km^R$ strain, confirming that the methylmalonyl-CoA pathway is essential for the assimilation of valerate.

The assimilation of propionyl-CoA yielded succinyl-CoA that can be converted into oxaloacetate and α -ketoglutarate using the oxidative and reverse TCA cycle, respectively. The assimilation of this C3 compound thus acts as an anaplerotic pathway. This keystone role in metabolism is commonly assumed by the EMC pathway in *Rs. rubrum*, but EMC has been shown to be non-essential under valerate condition. Our results also revealed that the pyruvate ferredoxin oxydoreductase, *rru_A2398*, was essential for phototrophic growth in the presence of valerate (Fig. 2, see supplementary table 3), indicating that acetyl-CoA could be converted into pyruvate, as this reaction is driven in this direction in an anaerobic environment (54). Moreover, we observed the essentiality of some enzymes of the BCAA biosynthesis pathway (Fig. 2, see supplementary table 3 and 4) for the photoheterotrophic assimilation of valerate, further corroborating the proteomic analysis and previous studies (11,12,14,15). The acetyl-CoA arising from the cleavage of valerate is thus redirected to other pathways than the EMC,

such as the BCAA biosynthesis pathway, PHA production or the PFOR. These pathways could help balance the redox pool state. Whereas the implication of PHA production in redox homeostasis is well accepted now, the involvement of the BCAA biosynthesis pathway as an electron sink is still controversial. However, this pathway has already been highlighted during the photoheterotrophic assimilation of other reduced VFAs, such as acetate (11), butyrate (14) or even after a sudden increase in light intensity (15). Altogether, the data obtained previously, and in this study, suggest that the BCAA biosynthesis pathway may act as another electron sink.

Regarding the present results, the 3-hydroxyvalerate monomers observed during PHA quantification could arise either from the condensation of acetyl-CoA and propionyl-CoA into 3-ketovaleryl-CoA and its further reduction into 3-hydroxyvaleryl-CoA or from the β -oxidation of valerate in which 3-hydroxyvalerate constitutes one intermediary. However, internal data show that the cultivation of *Rs. rubrum* in the presence of acetate and propionate led to the production of PHA containing a reduced percentage of 3-hydroxyvalerate monomer (unpublished data). Moreover, the cultivation of *Rs. rubrum* in the presence of hexanoate led to the incorporation of 3-hydroxyhexanoate in the polymer, which is not observed in the presence of acetate or butyrate, further suggesting that at least a part of the carbon source is directly incorporated into the polymer(66).

3.4 Polyhydroxyalkanoate characterization reveals the production of the copolymer poly(3-hydroxybutyrate-co-3-hydroxyvalerate)

The use of carbon sources with an odd number of carbon has been linked to the production of copolymers of poly(3-hydroxybutyrate-co-3-hydroxyvalerate) exhibiting outstanding physicochemical properties(28,67–70). PHA quantitation has already revealed a higher production of PHAs in the presence of valerate compared to succinate. Interestingly,

the PHAs produced are copolymers of poly(3-hydroxybutyrate-co-3-hydroxyvalerate) (P(HB-co-HV)) with high monomeric percentage of 3-hydroxyvalerate ($83.90 \pm 4.19\%$ of the total polymer) (Fig. 3A). Even though this HV monomer percentage has already been observed using an engineered strain of *E. coli* in which the gene coding for the propionyl-CoA transferase was introduced (71), we have now observed this percentage in a wild-type strain (17,21,52). Moreover, it is interesting to note that cultivating *Rs. rubrum* in a bicarbonate ions limiting condition, which allowed the total PHA content of biomass to be increased, had no significant impact on the 3-HV content (Fig. 3B). The chemical and mechanical properties or biodegradability of PHAs are dependent on their monomeric composition, as well as on how they are concatenated (67,72,73). In this context, we attempted to control *Rs. rubrum* copolymer production by cultivating *Rs. rubrum* in the presence of acetate as the sole source of carbon (124 mM C equivalent) and we added 10 mM of valerate (50 mM C equivalent) when the culture reached mid-log phase ($DO_{680nm} \sim 2.0$). Whereas the HV content was negligible before valerate addition, the HV monomer accumulated quickly in the PHA polymer reaching $7.02 \pm 1.04\%$ of CDW only 11 hours after the addition of valerate in the medium, corresponding to a monomeric content of $14.51 \pm 2.41\%$ of the total PHA (Fig. 5). This result suggests that the production of PHA might be controlled by the sequential addition of the suitable VFA in order to design the desired copolymer for defined applications.

4. Conclusion

We have demonstrated here that the presence of HCO_3^- is mandatory for the photoheterotrophic assimilation of valerate. We have shown that the requirement of HCO_3^- was driven to the CBB cycle in order to regulate the redox balance (*i.e.* highly reduced carbon source and phototrophic metabolism). We have highlighted that following its activation in valeryl-CoA, valerate was cleaved into acetyl-CoA and propionyl-CoA. Whereas, the

483 ethylmalonyl-CoA pathway was not essential for the assimilation of valerate, a functional
484 methylmalonyl-CoA pathway was mandatory. We observed polyhydroxyalkanoate production
485 during photoheterotrophic metabolism of valerate that is undoubtedly used as an electron sink
486 and that can reach up to 15% of the cell dry weight as PHA. Using a knowledge based
487 optimization process, we have improved the yield of this production to achieve a PHA content
488 of more than 22% of the biomass by cultivating the bacteria in bicarbonate ion limiting
489 conditions, which further reduced the activity of another electron sink, the Calvin-Benson-
490 Bassham cycle. This type of observation has already been emphasized by our research group
491 following a sudden increase in light intensity. Finally, the characterization the PHA produced
492 revealed an outstanding proportion of 3-hydroxyvalerate monomer content. Moreover, we
493 have displayed the possibility of controlling the monomeric microstructural composition of
494 PHA by sequentially adding the wanted VFA in order to produce the most suitable polymer.

495 **5. Data availability statement**

496 The datasets generated for this study can be found on MassIVE repository (dataset
497 identifier: MSV000085300)

498 (<https://massive.ucsd.edu/ProteoSAFe/dataset.jsp?task=b5561aeb53f940248f6032205e12e014>).

499

6. Figure legends

Fig. 1:

(A) Growth of *Rs. rubrum* under succinate low HCO_3^- concentration (o) and valerate low (\square) and high (Δ) concentration of HCO_3^- . (B) Growth of *Rhodospirillum rubrum* in the presence of succinate (o) and valerate (\square) with a pulse of 10 mM bicarbonate ions. n=5

Fig. 2:

Schematic representation of the central carbon metabolism with proteins implicated in valerate assimilation as highlighted by proteomic data. The colored squares indicate fold change between valerate and succinate condition ranging from red (proteins are less abundant in the valerate condition) to green (proteins are more abundant in the valerate condition). Non-significant proteins are represented by stripped markers. Peptide number used to identify the protein is represented next to the marker. Colored circles indicate essentiality of gene based on fitness values obtained during mutant fitness assay n=5

Fig. 3:

Rs. rubrum growth (upper figures) and PHA production (lower figures) observed in the presence of (A) valerate +50 mM HCO_3^- and (B) valerate + progressive addition of 3 mM bicarbonate ions (vertical dotted lines). 3-hydroxybutyrate (dark grey) and 3-hydroxyvalerate (light grey) monomers content was determined through GC-MS analysis. n=5

Fig. 4:

(A) Growth of *Rs. rubrum* wild-type strain in the presence of succinate (o) or valerate (Δ) as the sole carbon source and $\Delta\text{ccr}::\text{Km}^R$ strain in the presence of valerate (\square) as the sole source of carbon. (B) Growth of *Rs. rubrum* wild-type strain in the presence of succinate (o) or valerate (Δ) as the sole carbon source and $\Delta\text{ccr}::\text{Km}^R$ strain in the presence of valerate (\square) as the sole source of carbon cultivated with the addition of 20mM of itaconic acid (B). n=5

Fig. 5:

Rs. rubrum growth and VFA consumption (upper figure) and PHA production (lower figure) observed in the presence of acetate (upper figure-full circle dotted line) and after a pulse of valerate (upper figure-open square dotted line-vertical dotted line). 3-hydroxybutyrate (dark grey) and 3-hydroxyvalerate (light grey) monomers content was determined through GC-MS analysis. n=5

7. Table legends

Table 1:

Proteins involved in the stress regulation and redox homeostasis highlighted by proteomic and mutant fitness analyses

8. Acknowledgement

This research was funded by the FRIA grant of Guillaume Bayon-Vicente (F.R.S-FRNS). This study was sponsored by the “Belgian Fund for Scientific Research (Grand equipment-F.R.S-FNRS).” The bioprofiling platform used for the proteomic analysis was supported by the European Regional Development Fund and the Walloon Region, Belgium.

G.B.V., B.L., and R.W. designed the study. G.B.V. and S.Z. performed the *Rs. rubrum* cultivation experiments. The mutant library construction was designed by A.D. and conducted by B.L. The mutant fitness assay was designed by G.B.V. and performed by G.B.V. A.D. carried out the BarSeq analysis. G.B.V. performed the bioinformatic analysis. G.B.V. and B.L. designed and performed the proteomic analysis. G.B.V. wrote the manuscript with the help of S.Z., B.L., A.D. and R.W.

9. References

- Hunter CN, Daldal F, Thurnauer MC, Beatty JT. The Purple Phototrophic Bacteria. Vol. 28. 2009.
- Tang KH, Tang YJ, Blankenship RE. Carbon metabolic pathways in phototrophic bacteria and their broader evolutionary implications. *Front Microbiol.* 2011;2(August):1–23.
- Tampio EA, Blasco L, Vainio MM, Kahala MM, Rasi SE. Volatile fatty acids (VFAs) and methane from food waste and cow slurry: Comparison of biogas and VFA fermentation processes. *GCB Bioenergy.* 2018;11(1):72–84.
- Paul S, Dutta A, Defersha F, Dubey B. Municipal Food Waste to Biomethane and Biofertilizer: A Circular Economy Concept. *Waste and Biomass Valorization.* 2018;9(4):601–11.
- Wainaina S, Awasthi MK, Sarsaiya S, Chen H, Singh E, Kumar A, et al. Resource recovery and circular economy from organic solid waste using aerobic and anaerobic digestion technologies. *Bioresour Technol* 2020;301(January):122778.
- Berg I a, Krasil’nikova EN, Ivanovsky RN. Investigation of the Dark Metabolism of Acetate in Photoheterotrophically Grown Cells of *Rhodospirillum rubrum*. *Microbiology.* 2000;69(1):7–12.
- Filatova L V., Berg I a., Krasil’nikova EN, Ivanovsky RN. A study of the mechanism of acetate assimilation in purple nonsulfur bacteria lacking the glyoxylate shunt: Enzymes of the citramalate cycle in *Rhodobacter sphaeroides*. *Microbiology.* 2005;74(3):265–9.
- Ivanovsky RN, Krasilnikova EN, Berg I a. A proposed citramalate cycle for acetate assimilation in the purple non- sulfur bacterium *Rhodospirillum rubrum*. *FEMS Microbiol Lett.* 1997;153:399–404.

- 570 9. Erb TJ, Fuchs G, Alber BE. (2S)- Methylsuccinyl-CoA dehydrogenase closes the ethylmalonyl-
571 CoA pathway for acetyl-CoA assimilation. *Mol Microbiol.* 2009;73(August):992–1008.
- 572 10. Erb TJ, Rétey J, Fuchs G, Alber BE. Ethylmalonyl-CoA mutase from *Rhodobacter sphaeroides*
573 defines a new subclade of coenzyme B12-dependent Acyl-CoA mutases. *J Biol Chem.*
574 2008;283(47):32283–93.
- 575 11. Leroy B, De Meur Q, Moulin C, Wegria G, Wattiez R. New insight into the photoheterotrophic
576 growth of the isocitrate lyase-lacking purple bacterium *Rhodospirillum rubrum* on acetate.
577 *Microbiology.* 2015;161:1061–72.
- 578 12. De Meur Q, Deutschbauer A, Koch M, Wattiez R, Leroy B. Genetic Plasticity and Ethylmalonyl
579 Coenzyme A Pathway during Acetate Assimilation in *Rhodospirillum rubrum* S1H under
580 Photoheterotrophic Conditions. 2018;84(3).
- 581 13. Kornberg H, Lascelles J. The formation of isocitratase by the *Athiorhodaceae*. *J Gen Microbiol.*
582 1960;23:511–7.
- 583 14. De Meur Q, Deutschbauer A, Koch M, Bayon-Vicente G, Cabecas Segura P, Wattiez R, et al.
584 New perspectives on butyrate assimilation in *Rhodospirillum rubrum* S1H under
585 photoheterotrophic conditions. *BMC Microbiol.* 2020
- 586 15. Bayon-vicente G, Wattiez R, Leroy B. Global Proteomic Analysis Reveals High Light Intensity
587 Adaptation Strategies and Polyhydroxyalkanoate Production in *Rhodospirillum rubrum*
588 Cultivated With Acetate as Carbon Source. *Front Microbiol.* 2020;11(March):1–17.
- 589 16. Albuquerque MGE, Eiroa M, Torres C, Nunes BR, Reis M a M. Strategies for the development
590 of a side stream process for polyhydroxyalkanoate (PHA) production from sugar cane
591 molasses. *J Biotechnol.* 2007;130:411–21.
- 592 17. Bengtsson S, Werker A, Christensson M, Welander T. Production of polyhydroxyalkanoates by
593 activated sludge treating a paper mill wastewater. *Bioresour Technol.* 2008;99:509–16.
- 594 18. Yoshikawa S, Araoka R, Kajihara Y, Ito T, Miyamoto H, Kodama H. Valerate production by
595 *Megasphaera elsdenii* isolated from pig feces. *J Biosci Bioeng.* 2018;125(5):519–24.
- 596 19. Hao J, Wang X, Wang H. Overall process of using a valerate-dominant sludge hydrolysate to
597 produce high-quality polyhydroxyalkanoates (PHA) in a mixed culture. *Sci Rep.* 2017;7(1):1–
598 11.
- 599 20. Janssen PH, Harfoot CG. Phototrophic growth on n-fatty acids by members of the family
600 *Rhodospirillaceae*. *Syst Appl Microbiol.* 1987;9(1–2):9–11.
- 601 21. Ho Gun Rhie, Dennis D. Role of *fadR* and *atoC*(Con) mutations in poly(3-hydroxybutyrate-Co-3-
602 hydroxyvalerate) synthesis in recombinant *pha+* *Escherichia coli*. *Appl Environ Microbiol.*
603 1995;61(7):2487–92.
- 604 22. Bugnicourt E, Cinelli P, Lazzeri a., Alvarez V. Polyhydroxyalkanoate (PHA): Review of synthesis,
605 characteristics, processing and potential applications in packaging. *Express Polym Lett.*
606 2014;8(11):791–808.
- 607 23. Urtuvia V, Villegas P, González M, Seeger M. Bacterial production of the biodegradable
608 plastics polyhydroxyalkanoates. *Int J Biol Macromol.* 2014;70:208–13.
- 609 24. Jeon JM, Brigham CJ, Kim YH, Kim HJ, Yi DH, Kim H, et al. Biosynthesis of poly(3-

- hydroxybutyrate-co-3-hydroxyhexanoate) (P(HB-co-HHx)) from butyrate using engineered *Ralstonia eutropha*. *Appl Microbiol Biotechnol*. 2014;98:5461–9.
25. Keshavarz T, Roy I. Polyhydroxyalkanoates: bioplastics with a green agenda. *Curr Opin Microbiol*. 2010;13(3):321–6.
26. Philip S, Keshavarz T, Roy I. Polyhydroxyalkanoates: biodegradable polymers with a range of applications. *J Chem Technol Biotechnol*. 2007;82(July 2006):1115–21.
27. Klask C, Raberg M, Heinrich D, Steinbuchel a. Heterologous Expression of Various PHA Synthase Genes in *Rhodospirillum rubrum*. *Chem Biochem Eng Q*. 2015;29(2):75–85.
28. Pardelha F, Albuquerque MGE, Reis MAM, Dias JML, Oliveira R. Flux balance analysis of mixed microbial cultures: Application to the production of polyhydroxyalkanoates from complex mixtures of volatile fatty acids. *J Biotechnol*. 1970;162(2–3):336–45.
29. Otzen C, Bardl B, Jacobsen ID, Nett M, Brock M. *Candida albicans* utilizes a modified β -oxidation pathway for the degradation of toxic propionyl-CoA. *J Biol Chem*. 2014;289(12):8151–69.
30. Snell KD, Feng F, Zhong L, Martin D, Madison LL. YfcX Enables Medium-Chain-Length Poly (3-Hydroxyalkanoate) Formation from Fatty Acids in Recombinant *Escherichia coli* fadB Strains. *Society*. 2002;184(20):5696–705.
31. Wetmore KM, Price MN, Waters RJ, Lamson JS, He J, Hoover CA, et al. Rapid Quantification of Mutant Fitness in Diverse Bacteria by Sequencing Randomly Bar-Coded Transposons. *MBio*. 2015;6(6):1–15.
32. Bradford MM. A rapid and sensitive method for the quantitation of microgram quantities of protein utilizing the principle of protein-dye binding. *Anal Biochem*. 1976;72(1–2):248–54.
33. Muller FM. On the metabolism of the purple sulphur bacteria in organic media. *Arch Mikrobiol*. 1933;4:131–66.
34. Laguna R, Tabita FR, Alber BE. Acetate-dependent photoheterotrophic growth and the differential requirement for the Calvin-Benson-Bassham reductive pentose phosphate cycle in *Rhodobacter sphaeroides* and *Rhodopseudomonas palustris*. *Arch Microbiol*. 2011;193:151–4.
35. Richardson DJ, King GF, Kelly DJ, Mcewan AG, Ferguson SJ, Jackson JB. The role of auxiliary oxidants in maintaining redox balance during phototrophic growth of *Rhodobacter capsulatus* on propionate or butyrate. 1988;2:131–7.
36. Rizk ML, Laguna R, Smith KM, Tabita FR, Liao JC. Redox homeostasis phenotypes in RubisCO-deficient *Rhodobacter sphaeroides* via ensemble modeling. *Biotechnol Prog*. 2011;27(1):15–22.
37. McKinlay JB, Harwood CS. Carbon dioxide fixation as a central redox cofactor recycling mechanism in bacteria. *Proc Natl Acad Sci U S A*. 2010;107(26):11669–75.
38. Porter J, Merrett MJ. Influence of Light Intensity on Reductive Pentose Phosphate Cycle Activity during Photoheterotrophic Growth of *Rhodospirillum rubrum* . *Plant Physiol*. 1972;50(2):252–5.
39. Gottschalk G. *Bacterial metabolism*, 2nd. 1986. 178–207 p.
40. Mckinlay JB, Harwood CS. Calvin Cycle Flux, Pathway Constraints, and Substrate Oxidation

- 650 State Together Determine the H₂ Biofuel Yield in Photoheterotrophic Bacteria. *MBio*.
651 2011;2:1–9.
- 652 41. Narancic T, Scollica E, Cagney G, O'Connor KE. Three novel proteins co-localise with
653 polyhydroxybutyrate (PHB) granules in *Rhodospirillum rubrum* S1. *Microbiol (United*
654 *Kingdom)*. 2018;164(4):625–34.
- 655 42. Handrick R, Reinhardt S, Schultheiss D, Reichart T, Schöler D, Jendrossek V, et al. Unraveling
656 the Function of the *Rhodospirillum rubrum* Activator of Polyhydroxybutyrate (PHB)
657 Degradation: The Activator Is a PHB-Granule-Bound Protein (Phasin). *J Bacteriol*.
658 2004;186(8):2466–75.
- 659 43. Hauf W, Schlebusch M, Hüge J, Kopka J, Hagemann M, Forchhammer K. Metabolic Changes in
660 *Synechocystis* PCC6803 upon Nitrogen-Starvation: Excess NADPH Sustains
661 Polyhydroxybutyrate Accumulation. *Metabolites*. 2013;3:101–18.
- 662 44. Jin H, Nikolau BJ. Role of genetic redundancy in polyhydroxyalkanoate (PHA) polymerases in
663 PHA biosynthesis in *Rhodospirillum rubrum*. *J Bacteriol*. 2012;194(20):5522–9.
- 664 45. Gordon GC, McKinlay JB. Calvin cycle mutants of photoheterotrophic purple nonsulfur
665 bacteria fail to grow due to an electron imbalance rather than toxic metabolite accumulation.
666 *J Bacteriol*. 2014;196(6):1231–7.
- 667 46. Narancic T, Scollica E, Kenny ST, Gibbons H, Carr E, Brennan L, et al. Understanding the
668 physiological roles of polyhydroxybutyrate (PHB) in *Rhodospirillum rubrum* S1 under aerobic
669 chemoheterotrophic conditions. *Appl Microbiol Biotechnol*. 2016
- 670 47. Cerrone F, Choudhari SK, Davis R, Cysneiros D, O'Flaherty V, Duane G, et al. Medium chain
671 length polyhydroxyalkanoate (mcl-PHA) production from volatile fatty acids derived from the
672 anaerobic digestion of grass. *Appl Microbiol Biotechnol*. 2014;98:611–20.
- 673 48. Santhanam A, Sasidharan S. Microbial production of polyhydroxy alkanotes (PHA) from
674 *Alcaligenes* spp . and *Pseudomonas oleovorans* using different carbon sources. *African J*
675 *Biotechnol*. 2010;9(21):3144–50.
- 676 49. Jendrossek D. Polyhydroxyalkanoate granules are complex subcellular organelles
677 (carbonosomes). *J Bacteriol*. 2009;191(10):3195–202.
- 678 50. Lee HOJ, Choi MH, Kim TUN, Yoon SC. Accumulation of Polyhydroxyalkanoic Acid Containing
679 Large Amounts of Unsaturated Monomers in *Pseudomonas fluorescens* BM07 Utilizing
680 Saccharides and Its Inhibition by 2-Bromooctanoic Acid. *Appl Environ Microbiol*. 2001;67(3–
681 12):4963–74.
- 682 51. Fradinho JC, Oehmen A, Reis MAM. Photosynthetic mixed culture polyhydroxyalkanoate (PHA)
683 production from individual and mixed volatile fatty acids (VFAs): Substrate preferences and
684 co-substrate uptake. *J Biotechnol*. 2014;185:19–27.
- 685 52. Page WJ, Manchak J, Rudy B. Formation of poly(hydroxybutyrate-co-hydroxyvalerate) by
686 *Azotobacter vinelandii* UWD. *Appl Environ Microbiol*. 1992;58(9):2866–73.
- 687 53. Jenkins LS, Nunn WD. Genetic and molecular characterization of the genes involved in short-
688 chain fatty acid degradation in *Escherichia coli*: the *ato* system. *J Bacteriol*. 1987;169(1):42–
689 52.
- 690 54. McNeely K, Xu Y, Ananyev G, Bennette N, Bryant DA, Dismukes GC. Characterization of a *nifJ*

- 691 mutant of *Synechococcus* sp. strain PCC 7002 lacking pyruvate:Ferredoxin oxidoreductase.
692 *Appl Environ Microbiol.* 2011;77(7):2435–44.
- 693 55. Tang KH, Yue H, Blankenship RE. Energy metabolism of *Heliobacterium modesticaldum* during
694 phototrophic and chemotrophic growth. *BMC Microbiol.* 2010;10.
- 695 56. Shimizu M, Fujii T, Masuo S, Takaya N. Mechanism of de novo branched-chain amino acid
696 synthesis as an alternative electron sink in hypoxic *Aspergillus nidulans* cells. *Appl Environ*
697 *Microbiol.* 2010;76(5):1507–15.
- 698 57. McCully AL, Onyeziri MC, LaSarre B, Gliessman JR, McKinlay JB. Reductive tricarboxylic acid
699 cycle enzymes and reductive amino acid synthesis pathways contribute to electron balance in
700 a *Rhodospirillum rubrum* Calvin-cycle mutant. *Microbiol Res.* 2020;
- 701 58. Savvi S, Warner DF, Kana BD, McKinney JD, Mizrahi V, Dawes SS. Functional characterization
702 of a vitamin B12-dependent methylmalonyl pathway in *Mycobacterium tuberculosis*:
703 Implications for propionate metabolism during growth on fatty acids. *J Bacteriol.*
704 2008;190:3886–95.
- 705 59. Williams DR, Anderson AJ, Dawes EA, Ewing DF. Production of a co-polyester of 3-
706 hydroxybutyric acid and 3-hydroxyvaleric acid from succinic acid by *Rhodococcus ruber*:
707 biosynthetic considerations. *Appl Microbiol Biotechnol.* 1994;40(5):717–23.
- 708 60. Carter MS, Alber BE. Transcriptional regulation by the short-chain fatty acyl coenzyme A
709 regulator (ScfR) PccR controls propionyl coenzyme A assimilation by *Rhodobacter*
710 *sphaeroides*. *J Bacteriol.* 2015;197(19):3048–56.
- 711 61. Haller T, Buckel T, Rétey J, Gerlt JA. Discovering new enzymes and metabolic pathways:
712 Conversion of succinate to propionate by *Escherichia coli*. *Biochemistry.* 2000;39(16):4622–9.
- 713 62. Macy JM, Ljungdahl LG, Gottschalk G. Pathway of succinate and propionate formation in
714 *Bacteroides fragilis*. *J Bacteriol.* 1978;134(1):84–91.
- 715 63. Koh A, De Vadder F, Kovatcheva-Datchary P, Bäckhed F. From dietary fiber to host physiology:
716 Short-chain fatty acids as key bacterial metabolites. *Cell.* 2016;165(6):1332–45.
- 717 64. Berg I a., Filatova L V., Ivanovsky RN. Inhibition of acetate and propionate assimilation by
718 itaconate via propionyl-CoA carboxylase in isocitrate lyase-negative purple bacterium
719 *Rhodospirillum rubrum*. *FEMS Microbiol Lett.* 2002;216:49–54.
- 720 65. Schneider K, Asao M, Carter MS, Alber BE. *Rhodobacter sphaeroides* uses a reductive route via
721 propionyl coenzyme A to assimilate 3-hydroxypropionate. *J Bacteriol.* 2012;194:225–32.
- 722 66. Cabecas Segura P, Obderwater R, Deutschbauer A, Dewasme L, Wattiez R, Leroy B. Unraveling
723 the production of poly(hydroxybutyrate-co-hydroxyhexanoate) and poly(hydroxybutyrate-co-
724 hydroxyvalerate-co-hydroxyhexanoate) in *Rhodospirillum rubrum*. *Prep.* 2020;
- 725 67. Žagar E, Kržan A, Adamus G, Kowalczyk M. Sequence distribution in microbial poly(3-
726 hydroxybutyrate-co-3-hydroxyvalerate) co-polyesters determined by NMR and MS.
727 *Biomacromolecules.* 2006;7:2210–6.
- 728 68. Venkateswar Reddy M, Venkata Mohan S. Effect of substrate load and nutrients
729 concentration on the polyhydroxyalkanoates (PHA) production using mixed consortia through
730 wastewater treatment. *Bioresour Technol.* 2012;114:573–82.

- 731 69. Brandl H, Knee EJ, Fuller RC, Gross R a., Lenz RW. Ability of the phototrophic bacterium
732 *Rhodospirillum rubrum* to produce various poly (3-hydroxyalkanoates): Potential sources for
733 biodegradable polyesters. *Int J Biol Macromol.* 1989;11:49–55.
- 734 70. Lemos PC, Serafim LS, Reis M a M. Synthesis of polyhydroxyalkanoates from different short-
735 chain fatty acids by mixed cultures submitted to aerobic dynamic feeding. *J Biotechnol.*
736 2006;122:226–38.
- 737 71. Yang YH, Brigham CJ, Song E, Jeon JM, Rha CK, Sinskey AJ. Biosynthesis of poly(3-
738 hydroxybutyrate-co-3-hydroxyvalerate) containing a predominant amount of 3-
739 hydroxyvalerate by engineered *Escherichia coli* expressing propionate-CoA transferase. *J Appl*
740 *Microbiol.* 2012;113(4):815–23.
- 741 72. Castro-Sowinski S, Burdman S, Matan O, Okon Y. Natural Functions of Bacterial
742 Polyhydroxyalkanoates. *Plast from Bact Nat Funct Appl.* 2010;14:121–32.
- 743 73. Sagong HY, Son HF, Choi SY, Lee SY, Kim KJ. Structural Insights into Polyhydroxyalkanoates
744 Biosynthesis. *Trends Biochem Sci.* 2018;43(10):790–805.

745

746

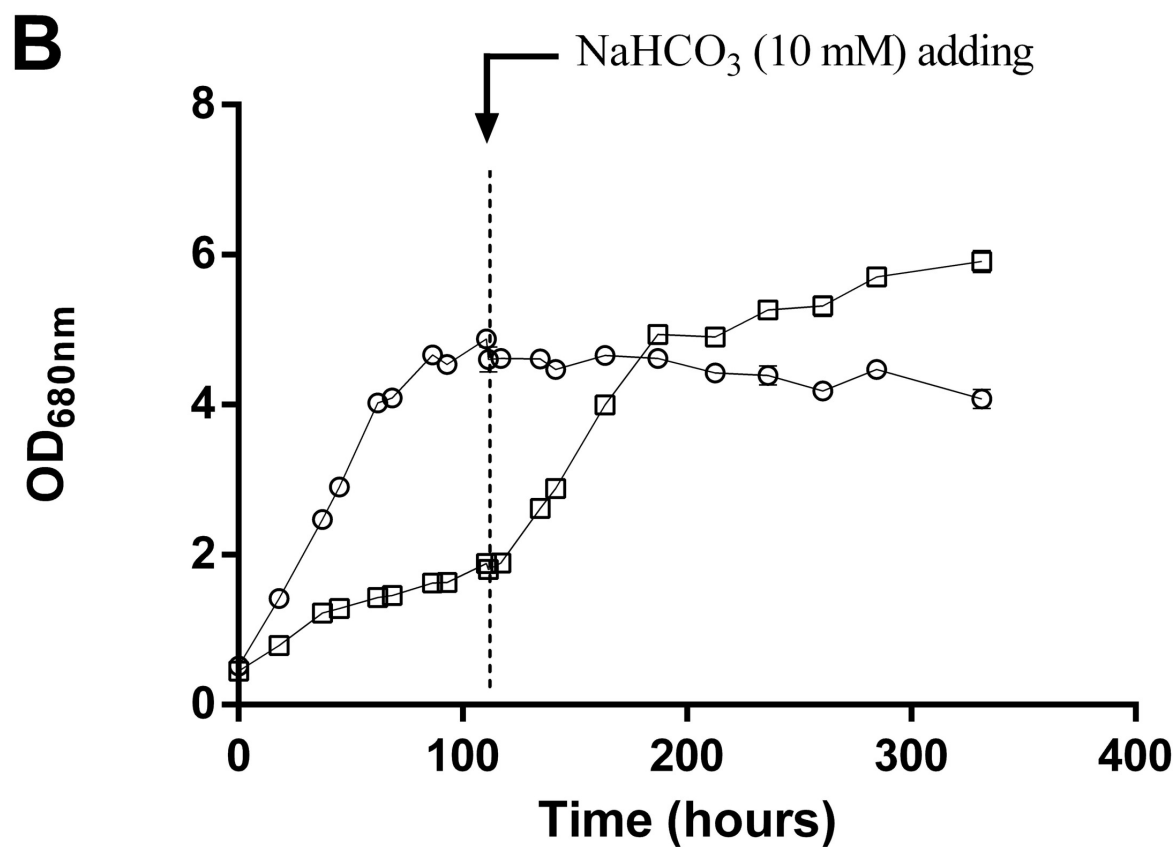
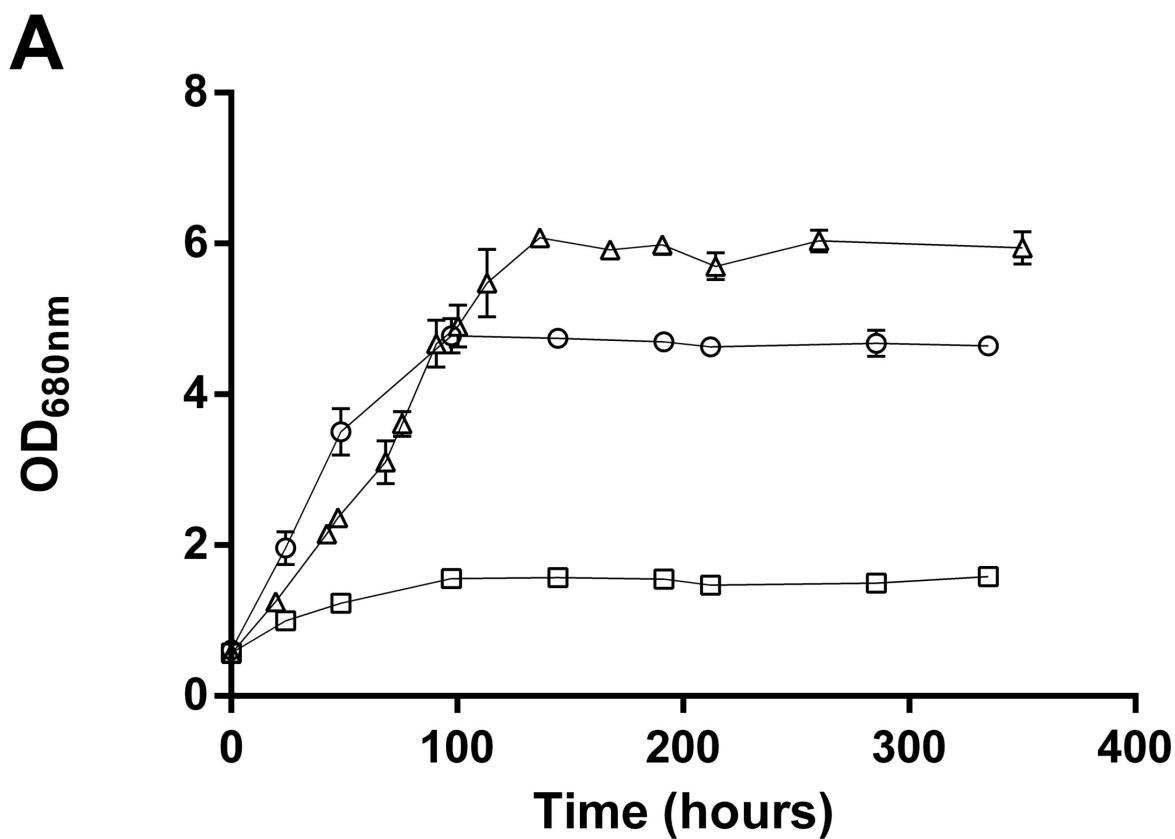
747

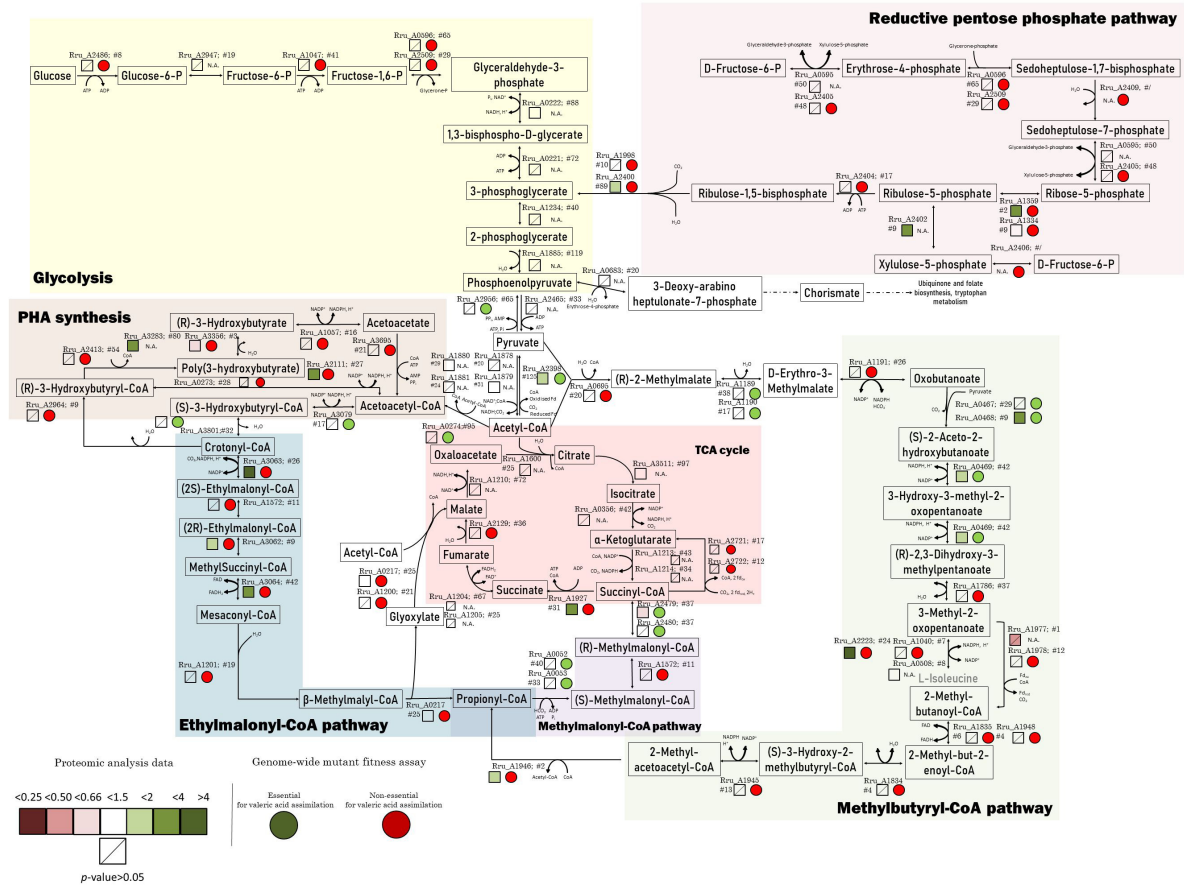
748

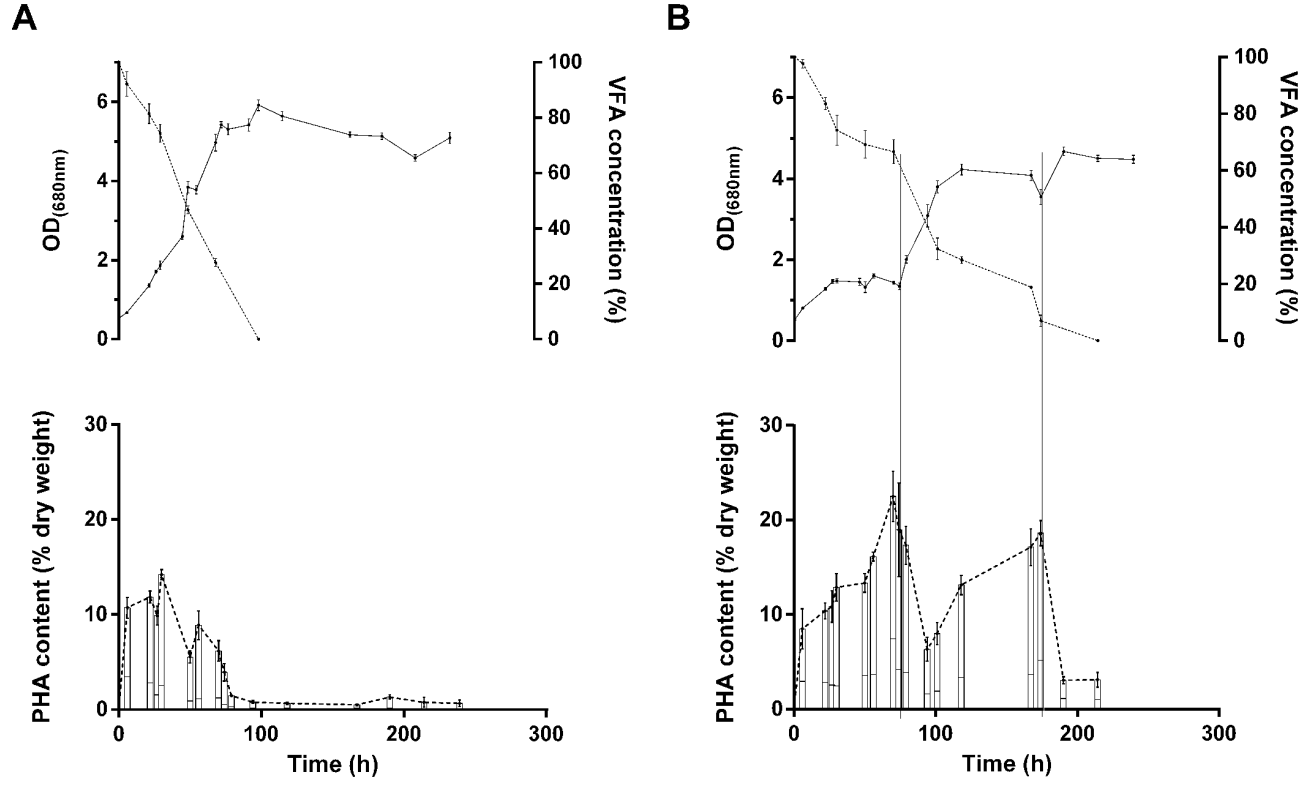
749

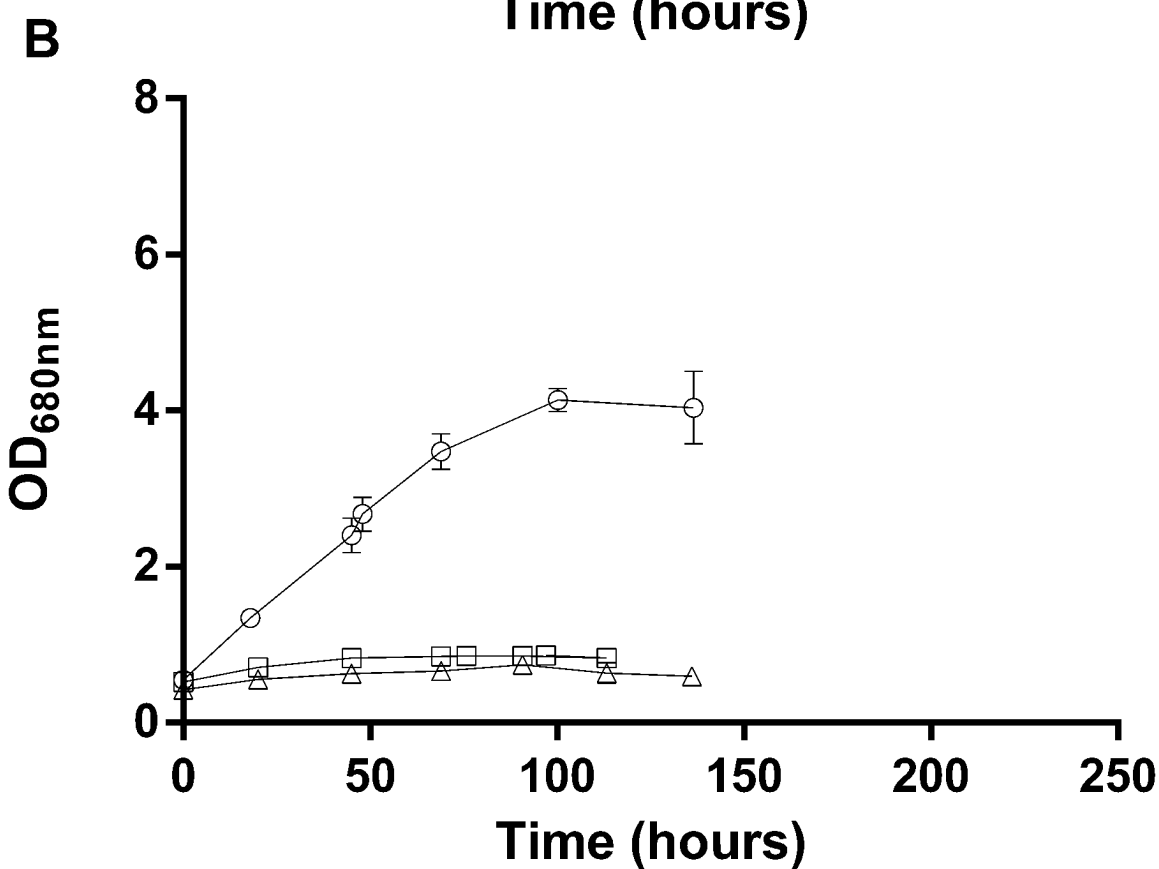
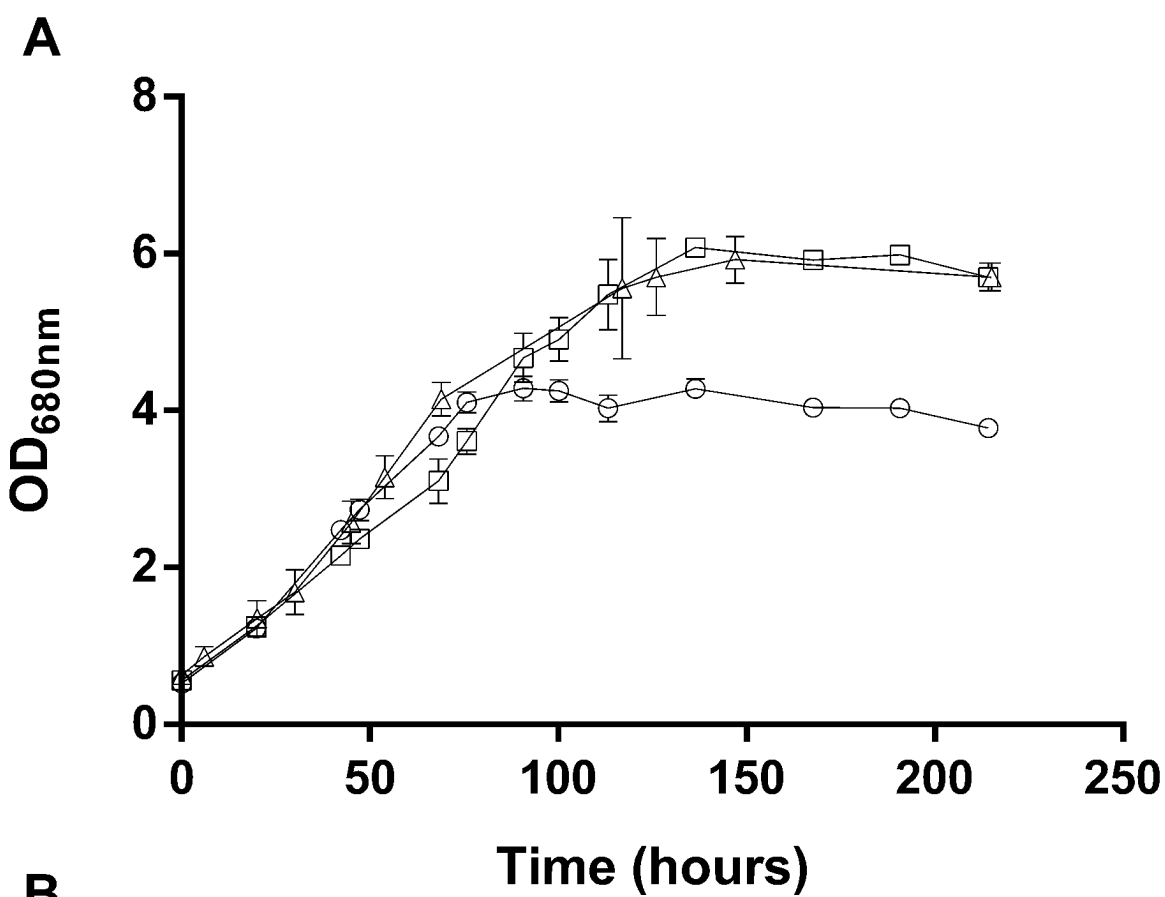
750

Peak Name	Locus Tag	Description	Proteomic analysis			Mutant fitness assay	
			<i>p</i> -value	Fold change Val/Succ	#Identified peptides	Fitness value Succinate	Fitness value Valerate
Stress handling and redox homeostasis							
Q2RW01	Rru_A0893	Stress protein	7.17E-03	2.00	41	N.A.	N.A.
Q2RW00	Rru_A0894	Stress protein	3.87E-02	1.91	78	-0.67	-1.24
Q2RUH6	Rru_A1418	Alkyl hydroperoxide reductase/ Thiol specific antioxidant/ Mal allergen	2.40E-03	1.60	42	N.A.	N.A.
Q2RTI5	Rru_A1760	Superoxide dismutase	5.30E-04	2.09	51	N.A.	N.A.
Polyhydroxyalkanoate metabolism							
Q2RXR6	Rru_A0274	Acetyl-CoA C- acetyltransferase	0.51	0.95	95	0.5	-2.4
Q2RSI4	Rru_A2111	Uncharacterised protein- potential phasin	2.24E-06	3.56	27	-0.44	0.37
Q2RQI1	Rru_A2817	Phasin	3.80E-04	48.24	24	-0.19	0.01
Q2RPS1	Rru_A3079	3-hydroxyacyl-CoA dehydrogenase	0.38	1.19	17	-0.3	-1.2
Q2RP67	Rru_A3283	Phasin	2.79E-02	2.06	80	N.A.	N.A.
Q2RNZ5	Rru_A3356	Polyhydroxyalkanoate depolymerase	4.14E-03	0.58	3	0.02	-0.28









VFAs concentration (mM of C)

